Molecular nanomagnets with competing interactions as optimal units for qudit-based quantum computation

M. Chizzini [1,2,*] L. Crippa [3,1,*] A. Chiesa [1,4,2] F. Tacchino [5] F. Petiziol [6] I. Tavernelli [5]
P. Santini [1,2,4] and S. Carretta [1,2,4,†]

[1]*Università di Parma, Dipartimento di Scienze Matematiche, Fisiche e Informatiche, I-43124 Parma, Italy*
[2]*INFN-Sezione di Milano-Bicocca, gruppo collegato di Parma, 43124 Parma, Italy*
[3]*IBM Italia S.p.a., Circonvallazione Idroscalo, 20090 Segrate, Italy*
[4]*UdR Parma, INSTM, I-43124 Parma, Italy*
[5]*IBM Quantum, IBM Research - Zurich, 8803 Rüschlikon, Switzerland*
[6]*Institut für Theoretische Physik, Technische Universität Berlin, Hardenbergstraße 36, 10623 Berlin, Germany*

Quantum systems displaying many accessible levels could be very powerful units of forthcoming quantum computing architectures. Indeed, the large number of available states could significantly simplify the actual implementation of several algorithms. Here we show that artificial molecular spins are particularly suitable to realize such a platform. In particular, multispin molecules with competing interactions provide a large number of low-energy multiplets in which decoherence is strongly suppressed compared to a single spin S and does not increase with the system size. This feature, combined with the proper connectivity between the multiplets, enables the implementation of complex operations with remarkable fidelity, thus fully unleashing the potential of the molecular approach. We demonstrate the power of this approach by numerically simulating the implementation of one- and two-qudit gates on realistic molecular systems.

I. INTRODUCTION

Molecular nanomagnets (MNMs) are very promising units for the design of quantum technologies [1] and in particular of quantum computing architectures [2–13]. These molecules, consisting of one or several interacting magnetic ions surrounded by organic ligand shells, can be manipulated by magnetic or electric pulses [14] and can be placed on surfaces [15,16] and in superconducting resonators [17], a state-of-the-art technology for quantum processors. In view of exploiting MNMs for quantum information processing, the prominent feature which makes them more attractive than most of the other established platforms is represented by their intrinsic multilevel structure. Indeed, MNMs are often characterized by many accessible low-energy levels with remarkable coherence [18,19], which can be exploited to encode information and to design algorithms based on a multilevel (qudit) logic [20,21]. In several cases, this may simplify the manipulation and control of quantum registers, allowing for compact encodings. Particularly in near-term architectures, these features could significantly ease the implementation of primitive algorithmic protocols [22–24], leading to effective realizations of digital quantum simulations [13,25,26] and quantum error correction [18,19,27,28].

Here we show how a proper hierarchy of spin-spin interactions in multispin clusters can significantly enhance the performance of molecular qudits in the implementation of complex gates. Indeed, MNMs with antiferromagnetic competing interactions between different ions [29–38] (labeled **C** in the following) are characterized by many low-spin multiplets in the bottom part of the spectrum, yielding a substantial suppression of decoherence [39], and by a high degree of connectivity between the eigenstates, leading to efficient decompositions of complex unitaries. We demonstrate the potential of this approach by numerically simulating the implementation of quantum gates on realistic **C** systems. We consider, in particular, an existing frustrated triangular Cu_3 qudit [40] and a model system consisting of a bipyramidal molecule, arranged as Ni_7 [41]. Other molecules with a similar structure also exist [42,43]. In both cases, the spectrum displays various low-spin multiplets at low energy. As a reference, we also examine isostructural molecules with ferromagnetic exchange interactions, leading to a ground multiplet behaving as a single spin S (**S** hereafter). Although chemically simpler, single-spin S molecules show a dramatically larger effect of decoherence and a reduced connectivity and they are, therefore, much less powerful. By comparing the two classes of systems, we demonstrate the striking advantage of **C** systems, which allows to significantly increase the working space dimension without increasing the effect of decoherence. The latter is included in all our simulations by considering the interaction of the molecular spins with a Markovian nuclear spin bath, the primary source of decoherence at low temperature.

*These authors contributed equally to this work.

†stefano.carretta@unipr.it

As a challenging test of our capability to achieve universal single-qudit control, we simulate a qudit Hadamard (H_d) gate, which effectively represents a Quantum Fourier Transform (QFT). Its implementation requires decomposition into several elementary operations, which by themselves would constitute a single-qudit universal set. In addition to that, we show how to extend our molecular setup to a multiqudit architecture, and we demonstrate how to implement switchable two-qudit controlled-phase gates. Combined with universal single-qudit operations, these constitute a universal set of gates.

Altogether, our results show that the possibility offered by MNMs to chemically tune their spin-spin couplings (a rather unique resource offered by these systems) makes them competitive not only with qudits characterized by a ladder connectivity between the levels (such as a spin-S ion), but also with standard multiqubits platforms.

The paper is organized as follows: We first introduce the model systems and describe decoherence. We then illustrate two different decompositions of a general unitary matrix on the qudit, with different requirements in terms of level connectivity. Next, we apply these decompositions to implement the H_d gate on the two classes of systems under investigation, i.e., multispin clusters with competing interactions and spin-S ions. We finally introduce a multiqudit architecture affording a switchable two-qudit gate which can be implemented on both kinds of compounds by means of simple semiresonant microwave pulses.

II. MODEL SYSTEMS AND DESCRIPTION OF DECOHERENCE

A. Multispin molecules with competing interactions

We consider N-spin molecules described by the following spin Hamiltonian:

$$\mathcal{H} = \sum_{i>j}^{N} J_{i,j} \mathbf{s}_i \cdot \mathbf{s}_j + \sum_{i>j}^{N} \mathbf{D}_{i,j} \cdot \mathbf{s}_i \times \mathbf{s}_j + \mu_B \mathbf{B}_0 \cdot \sum_i^{N} \mathbf{g}_i \cdot \mathbf{s}_i,$$

(1)

where $\mathbf{s}_i$ are spin operators; the first term is the leading one and represents the isotropic exchange interaction between different ions (with couplings $J_{i,j}$), the second is the Dzyaloshinskii-Moriya interaction (DMI) with coupling $\mathbf{D}_{i,j}$, and the last is the Zeeman interaction of each ion with an external magnetic field $\mathbf{B}_0$, parametrized by tensors $\mathbf{g}_i$. The aim of the work is to show that competing antiferromagnetic interactions are a key ingredient in designing optimal molecular qudits. Hence, we focus on two examples: the existing Cu_3 spin triangle (**C**1) studied in Refs. [40,44] and sketched in the inset of Fig. 1(a), one of the simplest molecules with competing interactions, and the hypothetical bipyramidal cluster (**C**2) shown in the inset of Fig. 1(b), whose structure is similar to Ni_7 molecules [41].

C1 consists of three $s_i = 1/2$ ions arranged in a practically isosceles triangle, with spin Hamiltonian parameters determined experimentally in Ref. [40]: $J_{12} = 0.390$ meV, $J_{13} = J_{23} = 0.348$ meV, $g_1^{xx} = g_1^{yy} = 2.2$, $g_2^{xx} = g_2^{yy} = 2.1$, $g_3^{xx} = g_3^{yy} = 2.4$, $g_i^{zz} = 2.0$, and $D_{12}^x = D_{12}^y = D_{12}^z = 0.045$ meV.
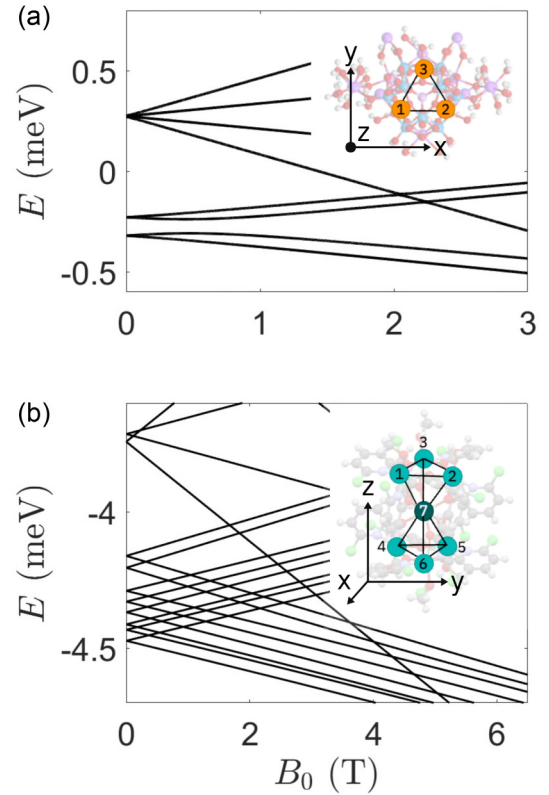

FIG. 1. Multispin molecules with competing interactions. Energy-level structure as a function of the external magnetic field of (a) system **C**1 and (b) system **C**2. The reference frame is oriented with the z axis exiting from the sheet (along the pyramidal axis). The external magnetic field is tilted with respect to the z axis in the xz plane of $\theta = 1$ rad ($\theta = 0$ rad). Insets: Scheme of the magnetic core of (a) **C**1 and (b) **C**2, with lines representing relevant interactions and the whole complex structure in transparency. System parameters are reported in the main text.

The other DMI couplings D_{ij}^α are obtained by applying D_{3h} symmetry to $\mathbf{D}_{12}$ (see Ref. [40] for details [45]). In the total spin basis $|S_{12}S\rangle$ (where $\mathbf{S}_{12} = \mathbf{s}_1 + \mathbf{s}_2$, $\mathbf{S} = \mathbf{S}_{12} + \mathbf{s}_3$) the isotropic exchange is diagonal and the energies of the multiplets can be analytically computed: $E(S_{12}, S) = S(S + 1)J_{13}/2 + S_{12}(S_{12} + 1)(J_{12} - J_{13})/2$. The resulting spectrum [reported as a function of B_0 in Fig. 1(a)] shows two low-energy doublets split by the difference between J_{12} and J_{13} and a higher-energy $S = 3/2$ multiplet which cross at rather high field. An anticrossing between the two doublets occurs at $B_0 \approx 0.8$ T due to the anisotropic DMI term ($\sim J_{i,j}/10$), which mixes the two multiplets. Here we have chosen the magnitude and orientation of the static magnetic field $B_0 = 1$ T, $\theta = 1$ rad [with respect to the z axis in the xz plane, as shown in the inset of Fig. 1(a)] in order to have well distinct energy gaps and sizable matrix elements between all the four states used to encode quantum information (see below).

As shown in the following sections, two key characteristics of optimal molecular qudits are the presence of many low-energy weakly magnetic eigenstates and the occurrence of sizable magnetic dipole matrix elements among most (or even all) of them. Indeed, the former mitigates decoherence and the latter enables one to efficiently manipulate the qudit

state with magnetic pulses. Therefore, we identify for the **C2** hypothetical system a regime of parameters leading to eight $S = 1/2$ multiplets in the bottom part of the spectrum [see level diagram in Fig. 1(b)]. This is achieved by using $s_i = 1/2$ for $i = 1, \ldots, 6$, $s_7 = 3/2$, isotropic exchange couplings $J_{i,7} = 0.95$ meV, $J_{1,2} = 1.29$ meV, $J_{2,3} = J_{3,1} = 1.25$ meV, $J_{4,5} = 1.41$ meV, and $J_{5,6} = J_{6,4} = 1.36$ meV, and isotropic g factors $g_1 = g_2 = g_4 = g_5 = 2.1$, $g_3 = g_6 = 2.15$, and $g_7 = 2$. These values are typical for Cu^{2+} (s_{1-6}) and Cr^{3+} (s_7) ions in a distorted octahedral crystal-field environment. We apply a magnetic field of 2.7 T along the z axis and for simplicity we consider only the z component of the DMI vector, $D_{i,j}^z = J_{i,j}/10$, a value close to those found experimentally on **C1**. Different choices of parameters (e.g., a different $\mathbf{D}_{i,j}$) fulfilling the same hierarchy do not qualitatively alter our conclusions (see below). In particular, the mixing between different S multiplets and hence the possibility to induce magnetic-dipole transitions between them only depends on the rank of the anisotropic interaction.

At low temperature, the leading error affecting the state of MNM qubits is represented by pure dephasing, induced by the coupling of the system spins with the surrounding nuclear spins, yielding a decay of the off-diagonal elements of the density matrix. This process involves only diagonal elements of local spin operators and hence it is not affected by connectivity. Conversely, phonon-mediated relaxation mechanisms are negligible. Indeed, phonon absorption is forbidden at low temperature and the probability of phonon emission (scaling as the third power of the energy gap) is also irrelevant because we focus on a set of states which are rather close in energy, whose gaps are much smaller than the Debye energy ($\geqslant 50$ K). This is also demonstrated by many experiments (see, e.g., Refs. [46–48]) showing that the relaxation time T_1 at low temperature becomes several orders of magnitude longer than the dephasing time T_2.

We consider here a Markovian bath and treat the dynamics of the system in the Lindblad approximation. A more complete description of the bath dynamics would be possible through computationally expensive many-body methods [28]. However, it would not qualitatively alter our conclusions on engineering the system Hamiltonian and eigenstates to suppress decoherence. Hence, we adopt a simplified picture, which is nevertheless able to capture all the essential ingredients [39]. Within the above approximations, the time evolution of the density matrix ρ is described by the equation (see Appendix A)

$$
\dot{\rho} = -i[\mathcal{H} + \mathcal{H}_1, \rho] + \sum_{\mu\nu} \Gamma_{\mu\nu}(2|\mu\rangle\langle\mu|\rho|\nu\rangle\langle\nu|
$$
$$
- \delta_{\mu\nu}|\mu\rangle\langle\mu|\rho - \delta_{\mu\nu}\rho|\nu\rangle\langle\nu|), \tag{2}
$$

where $|\mu\rangle$, $|\nu\rangle$ are system eigenstates; the first term represents the coherent Hamiltonian evolution (including driving pulses $\mathcal{H}_1$), while the second one models pure dephasing. This yields an independent decay of each off-diagonal element $\rho_{\mu\nu}$ of the density matrix with a rate $\gamma_{\mu\nu} = \Gamma_{\mu\mu} + \Gamma_{\nu\nu} - 2\Gamma_{\mu\nu}$. The coefficients $\Gamma_{\mu\nu}$ are computed from the molecular structures

shown in the insets of Fig. 1 as follows:

$$
\Gamma_{\mu\nu} = \sum_{jj'=1}^{N} \sum_{\substack{\alpha\alpha'=\\x,y,z}} C_{jj'}^{\alpha\alpha'} \langle\mu|s_j^\alpha|\mu\rangle\langle\nu|s_{j'}^{\alpha'}|\nu\rangle, \tag{3}
$$

where $C_{jj'}^{\alpha\alpha'} = \sum_{nn'} \sum_{\beta\beta'} \chi_{nn'}^{\beta\beta'}(0) d_{jn}^{\alpha\beta} d_{j'n'}^{\alpha'\beta'}$, $\chi_{nn'}^{\beta\beta'}(0)$ is the zero-energy bath spectral function (see Appendix A), and $d_{jn}^{\alpha\beta}$ are components of the dipole-dipole interaction tensor between the jth electronic spin and the nth nuclear spin, computed in the point-dipole approximation. For isotropic nuclear magnetic moments, these are given by

$$
d_{jn}^{\alpha\beta} = \frac{\mu_B \mu_N g_N}{R_{jn}^3} \left[g_j^{\alpha\beta} - 3\frac{R_{jn}^\beta \left(\sum_\gamma g_j^{\alpha\gamma} R_{jn}^\gamma\right)}{R_{jn}^2} \right], \tag{4}
$$

where g_N is the nuclear g factor, μ_N is the nuclear magneton, and R_{jn}^α is the α component of the distance between the jth electronic spin and the nth nuclear spin. We stress that we consider the real positions of nuclear spins taken from published molecular structures, both for Cu_3 [44] and for the double tetrahedron, in which case we consider the structure of Ni_7 [49].

Dephasing resulting from Eq. (3) is driven by differences between the expectation values of local spin operators s_j^α on pairs of eigenstates $|\mu\rangle$, $|\nu\rangle$. Hence, apart from the specific distribution of nuclei determining the coefficients $C_{jj'}^{\alpha\alpha'}$, decoherence depends crucially on the spin structure of the eigenstates. The latter is mainly determined by the pattern of isotropic exchange couplings and depends weakly on the specific form of the DMI. For instance, we have checked that by changing $\mathbf{D}_{i,j}$ from $D_{i,j}^z\hat{\mathbf{z}}$ to $D_{i,j}^z(\hat{\mathbf{x}} + \hat{\mathbf{y}} + \hat{\mathbf{z}})/\sqrt{3}$ the average $\bar{\Gamma} = \sum_{\mu\nu} \Gamma_{\mu\nu}/d^2$ only changes by $\sim 10\%$.

Even though all the following simulations have been performed using the full Eq. (3), an intuitive picture of how the form of the eigenstates affects decoherence can be gained by considering the limiting case of (i) all the nuclear spins very far away from the system spins and (ii) $\langle\mu|S_\alpha|\mu\rangle \propto \delta_{\alpha z}$, as for an axial Hamiltonian with the magnetic field along z (here $S_\alpha = \sum_j s_j^\alpha$). In that situation $C_{jj'}^{\alpha\alpha'}$ is independent on j, j', $\Gamma_{\mu\nu}$ simplifies into $\Gamma_{\mu\nu} \propto \langle\mu|S_z|\mu\rangle\langle\nu|S_z|\nu\rangle$, and the decay rates $\gamma_{\mu\nu}$ become $\propto (\langle\mu|S_z|\mu\rangle - \langle\nu|S_z|\nu\rangle)^2$. In this limiting case, subspaces characterized by the same $\langle S_z\rangle$ are decoherence free. In general, this suggests that systems with competing interactions, whose eigenstates are characterized by small total spin S and small differences in the expectation values of s_j^α, are substantially protected from decoherence. Therefore, to study the suppression of decoherence which can be achieved by proper choice of the spin system, we perform the full calculation outlined above comparing **C1** and **C2** with another class of compounds, displaying a very different structure of the eigenstates, namely, a spin-S ground multiplet.

B. Spin-S system

The simplest molecular spin qudit is a compound containing a single magnetic ion with spin $S > 1/2$. Hence, it is worth investigating also this class of compounds to compare their computational capabilities with that of the multispin systems presented above. We describe S systems by means of the

following Hamiltonian:

$$\mathcal{H}_S = DS_z^2 + g\mu_B B_0 S_z, \tag{5}$$

where for simplicity we have assumed parallel axial anisotropy and magnetic field orientation [50]. $\mathcal{H}_S$ and S_z share a common basis of eigenstates $|m\rangle$, such that $S_z|m\rangle = m|m\rangle$. In the following simulations, we have assumed typical parameters [47,51] for (i) an $S = 3/2$ ion such as Cr^{3+} in an octahedral crystal field (**S1**), i.e., $D = 30$ µeV and $g = 1.98$; (ii) an $S = 5/2$ ion such as Mn^{2+} or Fe^{3+} in the same ligand cage (**S2**), namely, $D = 30$ µeV and $g = 2.0$; and (iii) an $S = 7/2$ ion such as Gd^{3+} (**S3**) [52], i.e., $D = 20$ µeV and $g = 2.0$.

As outlined above, two main ingredients contribute to the dephasing time of a molecular spin system: the structure of the eigenstates and its coupling to the nuclear spin bath. Here we want to focus on the former and identify general properties which can be exploited at the synthetic level to suppress pure dephasing. Thus, we need to keep the positions of nuclear and system spins fixed when comparing **C** and **S**. Hence, we consider two isostructural molecules in which the sign of the isotropic exchange is reversed. In this way, the dipolar couplings between system and bath spins are exactly the same, while the structure of the eigenstates changes dramatically. In particular, a multispin molecule in which ferromagnetic exchange is the leading interaction is characterized by a ground multiplet with total spin $S = \sum_{i=1}^{N} s_i$, independently from the values of $J_{i,j} < 0$. This spin-S ground multiplet is characterized by the same $|m\rangle$ eigenstates of a single spin-S ion, although we have started from the molecular structure of **C**. This allows us to make a direct comparison between **S** and **C** and to ascribe the whole difference to the composition of the eigenstates.

We can now easily compute $\langle m|s_j^\alpha|m\rangle$ entering Eq. (3). Thanks to the Wigner-Eckart theorem [53] and to axial symmetry, within a spin-S multiplet with small anisotropy we get $\langle m|s_j^\alpha|m\rangle = \zeta_j \langle m|S_z|m\rangle \delta_{\alpha z}$. Then, one finds

$$\Gamma_{mm'}^{\mathbf{S}} = \left(\sum_{jj'} C_{jj'}^{zz} \zeta_j \zeta_{j'} \right) mm' = \frac{mm'}{T_2}, \tag{6}$$

where we have introduced an effective dephasing rate $T_2^{-1} = \bar{\chi} \sum_{jj'} c_{jj'}^{zz} \zeta_j \zeta_{j'}$ containing all the information about the nuclear spin bath, namely, the distribution of nuclei and the (unknown) bath spectral functions $\chi_{nn'}^{\beta\beta'}$. For the sake of simplicity, here we have approximated $\chi_{nn'}^{\beta\beta'}$ as a constant $\bar{\chi}$ and we have factorized it from the geometric factor $c_{jj'}^{zz}$. Note that $\bar{\chi}$ is the same for both **S** and **C**. Hence, we rewrite Eq. (3) also for systems **C** in terms of the dephasing time T_2, i.e.,

$$\Gamma_{\mu\nu}^{\mathbf{C}} = \frac{1}{T_2 \sum_{jj'} c_{jj'}^{zz} \zeta_j \zeta_{j'}} \sum_{\substack{jj'=1 \\ \alpha\alpha'}}^{N} c_{jj'}^{\alpha\alpha'} \langle \mu|s_j^\alpha|\mu\rangle \langle \nu|s_j^{\alpha'}|\nu\rangle, \tag{7}$$

where only T_2 and the geometric factors $c_{jj'}^{\alpha\alpha'} = \sum_{nn'} \sum_{\beta\beta'} d_{jn}^{\alpha\beta} d_{j'n'}^{\alpha'\beta'}$ appear.
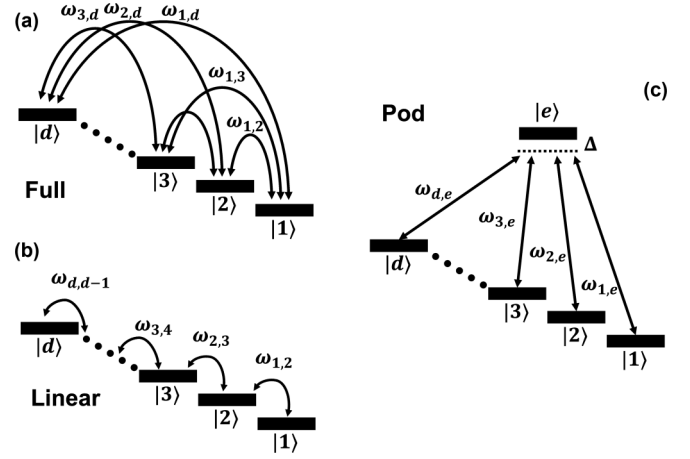

FIG. 2. Interlevel connectivity in qudit system, enabling different decompositions of a general d-dimensional unitary matrix. (a) "Full" connectivity among all the logical states, (b) "linear" connectivity between consecutive levels, and (c) "pod" connectivity required by the quantum Householder reflection, with an auxiliary level $|e\rangle$. On systems characterized by (a) and (b) we apply the decomposition in planar rotations. The frequency of the pulses used to implement PRs and QHRs is indicated by $\omega_{\mu\nu}$ for addressing the pair of $|\mu\rangle$ and $|\nu\rangle$ eigenstates.

III. DECOMPOSITION METHODS

A universal quantum gate set on a multiqudit system can be obtained by combining single-qudit rotations and a suitable entangling two-qudit operation. We will address two-qudit gates in Sec. V below. As far as single-qudit gates are concerned, several ways of factorizing a generic unitary on a d-dimensional qudit into a sequence of elementary transformations are known [22,54]. A minimal set is given, for instance, by Givens rotations between pairs of consecutive energy levels [55–57], also known as planar rotations (PRs) in the context of quantum optimal control theory [58]. These are $d \times d$ matrices $U_{\mu\nu}(\theta, \beta)$ given by

$$
\begin{aligned}
U_{\mu\nu}(\theta, \beta) &= \cos(\theta/2)(|\mu\rangle\langle\mu| + |\nu\rangle\langle\nu|) \\
&\quad + \sin(\theta/2)(|\nu\rangle\langle\mu|e^{i\beta} - |\mu\rangle\langle\nu|e^{-i\beta}) \\
&\quad + \sum_{\ell \neq \mu, \nu} |\ell\rangle\langle\ell|,
\end{aligned}
\tag{8}
$$

i.e., equal to the identity except for the elements in the intersection between the μth and νth rows and columns. A decomposition in PRs can be applied to any quantum system (e.g., both to **S** and **C**) with matrix elements enabling transitions induced by electromagnetic pulses at least between consecutive energy levels [as in Fig. 2(b)].

A larger number of allowed transitions (i.e., a higher connectivity) will make the decomposition more efficient, as discussed below. In particular, the connectivity between energy levels obtained in **C** enables us to adopt a more efficient decomposition scheme for an arbitrary transformation: the quantum Householder reflections (QHRs), presented in Sec. III B.

A. Planar rotations

As detailed in Appendix B, a general $W \in SU(d)$ can be decomposed in PRs as follows:

$$
\begin{aligned}
W = \Lambda & \left(e^{i\alpha_1}, e^{i\alpha_2}, \ldots, e^{i\alpha_{d-1}}, e^{-i\sum_{k=1}^{d-1}\alpha_k} \right) \\
& \times U_{1,2}(\theta_1, \beta_1) U_{1,3}(\theta_2, \beta_2) U_{2,3}(\theta_3, \beta_3) \ldots \\
& \times U_{1,d}\left(\theta_{\frac{(d-1)(d-2)}{2}+1}, \beta_{\frac{(d-1)(d-2)}{2}+1} \right) \\
& \times U_{2,d}\left(\theta_{\frac{(d-1)(d-2)}{2}+2}, \beta_{\frac{(d-1)(d-2)}{2}+2} \right) \ldots \\
& \times U_{d-1,d}\left(\theta_{\frac{d(d-1)}{2}}, \beta_{\frac{d(d-1)}{2}} \right)
\end{aligned} \tag{9}
$$

where Λ is a diagonal matrix with the elements shown in brackets. Notice that each PR [Eq. (8)] between a pair of eigenstates $|\mu\rangle$ and $|\nu\rangle$ connected by a dipole matrix element ($\propto \sum_j g_j^\alpha s_j^\alpha$) is implemented by a transverse magnetic pulse resonant with the corresponding transition. The diagonal matrix Λ is decomposed into a sequence of phase gates $P_{\mu\nu}(\alpha)$:

$$
P_{\mu\nu}(\alpha) = |\mu\rangle\langle\mu|e^{i\alpha} + |\nu\rangle\langle\nu|e^{-i\alpha} + \sum_{\ell \neq \mu, \nu} |\ell\rangle\langle\ell|. \tag{10}
$$

Each $P_{\mu\nu}(\alpha)$ is implemented by a semiresonant pulse between pairs of eigenstates $|\mu\rangle$ and $|\nu\rangle$ [25].

The decomposition shown in Eq. (9) can be always adopted, given the matrix element between states $|\mu\rangle$ and $|\nu\rangle$ needed to implement each $U_{\mu\nu}$. This can be straightforwardly applied to systems characterized by all-to-all connectivity between the energy levels, as shown in Fig. 2(a). If the direct transition $|\mu\rangle \to |\nu\rangle$ is not allowed, $U_{\mu\nu}$ can be further decomposed into available transitions by additional π pulses. For instance, in systems characterized by linear connectivity such as **S** [Fig. 2(b)], only transitions between consecutive levels $|m\rangle \leftrightarrow |m \pm 1\rangle$ are permitted. Hence, $U_{mm'}$ rotations for pairs of states $|m - m'| > 1$ must be further broken up into $U_{m,m\pm 1}$ by additional π pulses to put $|m\rangle$ and $|m'\rangle$ close, thus increasing the length of the pulse sequence. The full sequences of pulses employed to decompose qudit Hadamard gates H_d are reported in Appendix B [59].

B. Quantum Householder reflections

In contrast to PR, QHR decomposition requires a "pod" connectivity between the energy levels, i.e., an auxiliary state $|e\rangle$ connected to all the states involved in the encoding [see Fig. 2(c)]. Remarkably, the DMI term in **C** can mix all the low-energy doublets, thus establishing a pod or even a full connectivity between the lowest eigenstates (depending on the relative orientation between $\mathbf{B}_0$ and $\mathbf{D}_{i,j}$). Hence, the proposed **C** systems support a QHR decomposition which significantly hastens the implementation of the gates (see below). Each step of the decomposition is represented by the so-called QHR, namely,

$$
M(v, \phi) = I + (e^{i\phi} - 1)|v\rangle\langle v|, \tag{11}
$$

where I is the identity matrix, $|v\rangle$ a d-dimensional normalized complex vector and ϕ an arbitrary phase. As described in Ref. [60] and in Appendix C, it is possible to analytically calculate the v_i and ϕ_i needed to decompose any unitary
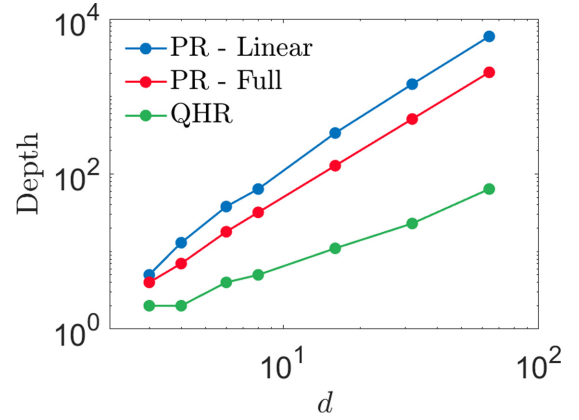

FIG. 3. Number of subsequent pulses (depth) required by the different decomposition schemes to decompose H_d as a function of the qudit space dimension d. We compare PRs on linearly (blue) or fully (red) connected systems and QHR (green) decompositions. All of them show a power scaling, with different exponent, the most efficient being QHR which requires at most $\sim d$ subsequent pulses (and even less for small d in the case of H_d). The PR method yields a $\sim \frac{d^2}{2}$ depth on a fully connected system (red), with an additional cost of $(d-1)(d-2)$ pulses in the case of linear connectivity (blue).

$W \in SU(d)$:

$$
W = \prod_{i=1}^{d} M(v_i, \phi_i). \tag{12}
$$

To implement the QHR $M_i = M(v_i, \phi_i)$ we use a set of simultaneous semiresonant transverse magnetic pulses [i.e., rectangular pulses detuned from the addressed gap by an amount Δ; see Fig. 2(c)] between each of the system eigenstates $|\mu\rangle$ and $|e\rangle$, with relative amplitude $\propto |\langle\mu|v_i\rangle|$ and phase $\arg\langle\mu|v_i\rangle$. All pulses begin and end simultaneously. The duration τ and the detuning Δ (common to all simultaneous pulses) depend on pulse amplitude and on ϕ_i according to

$$
\tau = \sqrt{\frac{\phi_i(2\pi - \phi_i)}{\Omega_{1e}^2 + \cdots + \Omega_{de}^2}},
$$
$$
\Delta = \pm \frac{\pi - \phi_i}{\tau}, \tag{13}
$$

where $\Omega_{\mu e}$ are the Rabi frequencies of the transitions.

As shown in Fig. 3 for a qudit Hadamard gate (see definition below), QHR allows us to drastically reduce the number of subsequent operations, leading to a circuit depth $\sim d$ (green symbols), as opposed to the $\sim d^2$ scaling obtained with PR (red and blue lines, considering full and linear connectivity between the levels, respectively).

IV. HADAMARD TRANSFORM ON OPTIMAL MOLECULAR QUDITS

Both PR and QHR decompositions, together with the connectivity between matrix elements shown in Fig. 2, allow one to build a general single-qudit unitary gate. As a prototypical test case, we consider here the qudit Hadamard gate (H_d). This

is defined by the following transformation:

$$\mathrm{H}_d = \frac{1}{\sqrt{d}} \sum_{\mu,\nu=1}^{d} e^{i\frac{2\pi}{d}(\mu-1)(\nu-1)} |\mu\rangle\langle\nu|, \qquad (14)$$

for a qudit of dimension d. It represents the quantum Fourier transform on a Hilbert space of dimension d, i.e., the same unitary that is usually implemented in multiqubit architectures on a set of $\log d$ qubits. The implementation of H_d is a very demanding benchmark of our capability to implement a general unitary gate, because its decomposition involves a large number of elementary steps, namely, PRs or QHRs. Hereafter, we show numerical simulations of the implementation of a Hadamard gate on $d = 4, 6, 8$ qudits defined in the basis of the lowest d system eigenstates of either systems with competing exchange interactions (**C1**,**C2**) or by single spin-S ions (**S1**, **S2**, **S3**).

A. Four-level qudits

We start from "small" $d = 4$ qudits and we compare the performance of the triangular Cu_3 system (**C1**), characterized by competing interactions, with a spin $S = 3/2$ ion (**S1**) such as Cr^{3+}. In **C1**, only the four states belonging to the two lowest doublets are considered.

Figure 4(a) shows the error $\mathcal{E} = 1 - \langle\psi|\rho|\psi\rangle$ after the implementation of an H_4 using PRs decomposition on both systems, as a function of the driving field amplitude B_1. Here ρ is the system density matrix at the end of the simulation and $|\psi\rangle = \mathrm{H}_d|\psi_0\rangle$ is the target state, $|\psi_0\rangle$ being the initial state. We consider a large range of driving fields, from 10 to 100 G, the maximum value available in state-of-the-art pulse electron paramagnetic resonance spectrometers [61]. We include the full sequence of rectangular pulses and the effect of decoherence with $T_2 = 3\,\mu s$ (solid circles) and $T_2 = 10\,\mu s$ (open circles). These numbers are perfectly realistic. Indeed, as experimentally demonstrated in Ref. [62], decoherence in **S** systems does not significantly depend on S, but only on Δm between the two states involved in the superposition (see Sec. II B). The here employed values of T_2 refer to single-quantum coherences ($\Delta m = \pm 1$) and hence we can take as reference the T_2 reported for $S = 1/2$ complexes, which have been much more studied and chemically optimized so far. In these cases, T_2 in the 10-μs range can be easily obtained by engineering the molecular structure [6,10,63], reaching even hundreds of microseconds [64,65]. Nevertheless, we remark that $T_2 \sim 2$–3 μs were already reported also for a Cr^{3+} complex with $S = 3/2$ and a Fe^{3+} compound with $S = 5/2$ at 5 K [62]. For multispin systems with competing interactions sharing the same nuclear spin bath, and a lack of experimental information, it is again reasonable to start from the same values.

The main figure shows results averaging on 30 configurations with different φ_μ phases of the initial state $|\psi_0\rangle = \sum_\mu e^{i\varphi_\mu}|\mu\rangle/\sqrt{d}$. This state is particularly error prone because it contains a uniform superposition of all the qudit eigenstates, which are therefore all subject to decoherence. The insets show an average over 30 different random initial states, displaying the same trend. At fixed B_1, the time required to implement the gate ($210 > t_{\mathrm{gate}} > 20$ ns) is very similar for
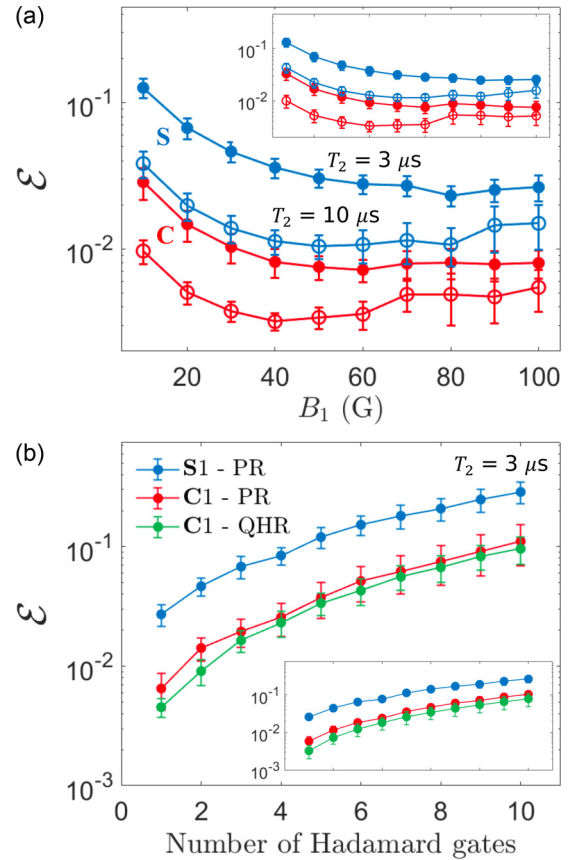

FIG. 4. (a) Error $\mathcal{E} = 1 - \langle\psi_0|\mathrm{H}_d^\dagger\rho\mathrm{H}_d|\psi_0\rangle$ after the implementation of a Hadamard gate on state $|\psi_0\rangle$ using PR decomposition on a $d = 4$ qudit represented by a Cu_3 (**C1**, red lines) or a Cr^{3+} spin $S = 3/2$ ion (**S1**, blue lines) as a function of the driving field amplitude B_1 and for two different T_2. Solid (open) circles have $T_2 = 3$ (10) μs. (b) Error $\mathcal{E}$ after the implementation of a sequence of Hadamard gates, using $T_2 = 3\,\mu s$ and $B_1 = 100$ G. For **C1** we show both PR and QHR decompositions, to implement H_4 and H_3, respectively, by exploiting the four lowest system eigenstates (for QHRs, the fourth state is the auxiliary $|e\rangle$). In the main panels we have considered 30 initial superpositions $|\psi_0\rangle = \sum_\mu e^{i\varphi_\mu}|\mu\rangle/\sqrt{d}$ with different phases φ_μ, while in the insets we have averaged over a set of 30 random initial states $|\psi_0\rangle$ with different amplitudes and phases, the error bars representing the standard deviation.

the two systems: indeed **C1** shows smaller transition matrix elements $|\langle\mu|\sum_j g_j^{xx} s_j^x|\nu\rangle|$, but the full connectivity ensures a more efficient decomposition, without additional π pulses.

For both examined systems, dephasing is the dominant issue, while pulse imperfections (yielding leakage to unwanted transitions) are found to be less important. Indeed, considering a $T_2 = 3\,\mu s$ the error $\mathcal{E}$ decreases almost monotonically as a function of B_1. The suppression of decoherence in **C1** leads to a remarkable reduction of $\mathcal{E}$ of a factor $\mathcal{R} \sim 3$–4 in the whole examined B_1 range. The gain $\mathcal{R}$ (i.e., the ratio between the error in **S1** and **C1**) is found to be practically independent from both B_1 and T_2.

Next, we consider the application of a sequence of H_4 gates. Figure 4(b) shows the results for both cases fixing $T_2 = 3\,\mu s$ and the driving field close to the corresponding optimal working point $B_1 = 100$ G. The advantage in using
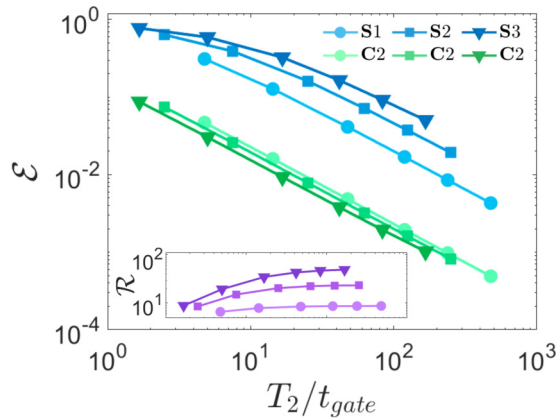
FIG. 5. Error in the implementation of H_4 (points), H_6 (squares), and H_8 (triangles) gates on **S**1, **S**2, **S**3 (blue tones), and **C**2 (green tones) systems (using $d = 4, 6, 8$ states for the encoding) as a function of T_2/t_{gate}. Inset: Gain ratio between errors on systems **S** and **C** using four- (circles), six- (squares) or eight-level (triangles) qudits. In these simulations leakage outside from the computational subspace is neglected and, to reduce the computational effort, we consider a single initial state $|\psi_0\rangle = \frac{1}{\sqrt{d}}\sum_l e^{i2\pi/\mu}|\mu\rangle$ where $\mu = 1, \ldots, d$ indicates the component of the $|\psi_0\rangle$ vector on the basis of the qudit eigenstates.

C1 remains even after application of up to 10 H_4, with an average $\mathcal{R} \sim 3.5$.

Here we also show an H_3 gate implemented by means of QHR decomposition (green), exploiting the three lowest levels for the logical qudit and the fourth as the auxiliary $|e\rangle$ in Fig. 2. The final error is further reduced, demonstrating the flexibility of **C**1 in efficiently allowing the implementation of both decompositions.

B. Larger qudits

Both the suppression of decoherence and the advantage of QHR decomposition are enhanced when the number of qudit levels, d, increases. We show this by focusing on the **C**2 system. We exploit its energy-level structure, displaying eight low-energy doublets, to define and manipulate qudits with a computational space dimension up to $d = 8$ (which could be further increased). In particular, the eight $m = -1/2$ states (one per each Kramers doublet), together with the first $m = +1/2$, offer the pod-system connectivity to implement gates using QHR decomposition. Magnetic dipole transitions between levels with $m = -1/2$ (defining the logical state) and the $m = +1/2$ level, which will be used as auxiliary $|e\rangle$, are all allowed due to intermultiplet mixing induced by DMI. In particular, the here considered axial DMI induces mixing only between states with $\Delta m = 0$ and hence a transverse oscillating field drives only $\Delta m = \pm 1$ transitions. This implies a pod connectivity (not full as in **C**1) between the lowest $d + 1$ levels, which is anyway sufficient to implement the QHR. Moreover, decoherence is strongly suppressed by choosing the eight logical states with the same $\langle S_z \rangle$.

Figure 5 shows the results of our simulations for implementing an H_d gate with $d = 4$ (points), $d = 6$ (squares), and $d = 8$ (triangles) comparing the performance of **C**2 (light, medium, and dark green) with that of **S**1 (light blue), **S**2

(medium blue), and **S**3 (dark blue). As done in the previous section, we initialize the systems into an error-prone state with the same absolute amplitude on each component, $|\psi_0\rangle = \sum_\mu e^{i\varphi_\mu}|\mu\rangle/\sqrt{d}$. We report simulation results in terms of T_2/t_{gate} using a weak oscillating field $B_1 = 10$ G, such that leakage becomes practically negligible. This choice is motivated by the fact that our focus here is on the impact of decoherence, and not on the effect of leakage. Indeed, pulse engineering [66–74] or quantum control techniques [75] could be used to significantly reduce it, but these methods are strongly system specific and computationally time-consuming. Hence, since we are dealing here with hypothetical systems, we prefer to neglect the use of weak driving fields and neglect the small amount of leakage to states above the lowest $d + 1$, thus making our results more general. For each series, we considered this list of values $T_2 = [1, 3, 10, 25, 50, 100]$ µs. As expected, system **C**2 with competing interactions is much less affected by decoherence, reaching $\mathcal{R} \sim 50$ for $d = 8$, as shown in the inset. Remarkably, in systems with competing interactions the effect of decoherence does not increase by increasing the number of levels. Indeed, green curves are practically superimposed. This removes the most important drawback of **S** systems, which instead show an error increasing with the number of levels in the encoding, and demonstrates the power of our optimization strategy.

Obviously, also t_{gate} is an important parameter to monitor. As before, the competing interaction system **C**2 compensates the reduction of the matrix elements exploiting the more efficient QHR decomposition, resulting in t_{gate} very similar to that obtained with PRs. For instance, H_4, H_6, and H_8 require about $t_{gate} = 200, 400$, and 600 ns, using a rather slow driving field of 10 G on average.

V. TWO-QUDIT GATES

In order to scale up the present molecular quantum hardware and complete the universal gate set, we now introduce a scheme to implement two-qudit entangling gates. To achieve this, we consider a pair of d-level qudits linked through an intermediate effective spin $1/2$, which acts as a switch of the qudit-qudit interaction [2,5,76,77], as shown in the inset of Fig. 6(a). The presence of a switch to dynamically turn on and off the effective qudit-qudit coupling is crucial to avoid unwanted two-qudit evolutions and hence enable the scalability of the architecture.

The spin Hamiltonian describing the two-qudit + switch system is the following:

$$\mathcal{H}_{2q} = \mathcal{H}_1 + \mathcal{H}_2 + \Delta\sigma_z/2 + \mathcal{H}_{1-\sigma} + \mathcal{H}_{2-\sigma}, \quad (15)$$

where $\mathcal{H}_{1,2}$ are the single-qudit Hamiltonians [either Eq. (14) or Eq. (5)], σ_α are Pauli matrices of the effective two-level switch, Δ is the switch splitting, and $\mathcal{H}_{i-\sigma}$ ($i = 1, 2$) is the qudit-switch coupling. In the case of **S** qudits, we assume $\mathcal{H}_{i-\sigma} = J_i \mathbf{S}_i \cdot \sigma$. For **C**1, we consider the coupling between each triangle and the switch via a single vertex, as shown in Fig. 7(a). Other choices of the coupling pattern or of the form (e.g., anisotropic) of the interaction lead to equivalent results. It is important to note that the precise values of the parameters entering Hamiltonian (15) are not important to realize our scheme and their precise optimization must be done after the
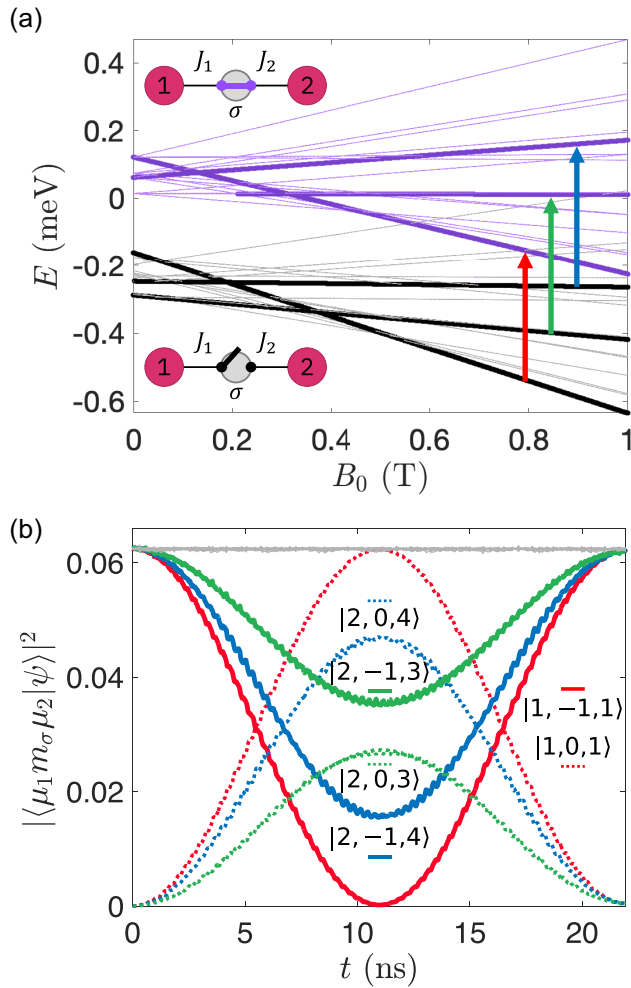
(a)

(b)

FIG. 6. (a) Energy levels of the selected two-qudit system composed by two $S = 3/2$ qudits and a $S = 1$ switch: black, energy levels with the switch spin expectation value -1; purple, 0. Thick levels are those involved in the transitions indicated by arrows and implemented in the simulation of the controlled-phase gate of panel (b). Upper (lower) inset: Sketch of the two-qudit system with the close (open) switch. System parameters: $D_1 = 30 \times 10^{-3}$ meV, $g_1 = 2.05$, and $J_1 = 5 \times 10^{-3}$ meV; $D_2 = 24 \times 10^{-3}$ meV, $g_2 = 1.95$, and $J_2 = 7 \times 10^{-3}$ meV. The spin-1 switch has $g_\sigma = 2.2$, and $d_\sigma = -0.3$ meV. (b) Simulated time evolution of the components of the two-qudit wave function during the implementation of the gate, implementing phases π, $\pi/2$, and $\pi/4$ to red, blue, and green levels, respectively. Gray lines represent the other energy levels of the system, not involved in the transitions, actually nonevolving. The initial state is uniformly populated, i.e., $|\psi_0\rangle = \sum_{\mu_1\mu_2} |\mu_1, m_\sigma = -1, \mu_2\rangle/d$ (where $d = 4$ is the qudit dimension). Reported simulations are performed using $B_1 = 20$ G as the maximum driving field amplitude.

synthesis of a suitable molecule. Our focus here is on the required hierarchy between different terms in $\mathcal{H}_{2q}$, which is crucial to guide future synthetic efforts.

Building a good switch requires factorization between qudit and switch states; i.e., the eigenstates must be close to $|\mu_1 m_\sigma \mu_2\rangle \equiv |\mu_1\rangle \otimes |m_\sigma\rangle \otimes |\mu_2\rangle$. Here we label as $|\mu_i\rangle$ the single-qudit eigenstates and with $|m_\sigma\rangle$ the eigenstates of the switch, corresponding to eigenstates of σ_z. Such a
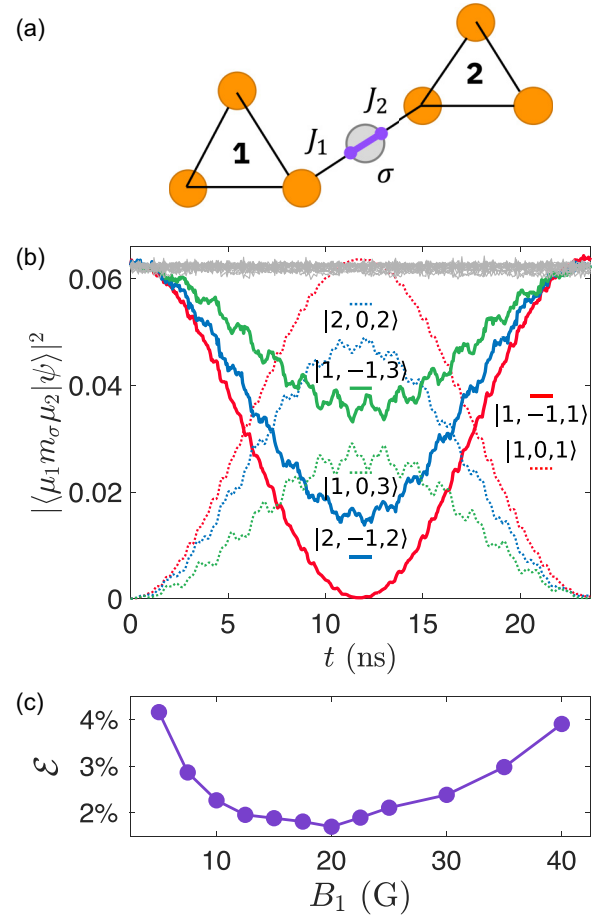
(a)

(b)

(c)

FIG. 7. (a) Sketch of the two-qudit system in which each unit consists of a **C**1 triangle. The two qudits are linked via a single vertex to an interposed Ni ion and rotated with respect to one another by 90° around y to make them inequivalent. (b) Time evolution of the components of the two-qudit wave function during the implementation of the gate, applying phases π, $\pi/2$, and $\pi/4$ to red, blue, and green levels, respectively. Solid and dotted lines represent state couples with the switch in ground and excited states. Gray lines represent the other energy levels of the system, not involved in the transitions, actually nonevolving. Reported simulations are performed using a driving field $B_1 = 20$ G as the maximum driving field amplitude. For the two qudits we use the same parameters as **C**1. We link them through a switch $g_\sigma = 2.2$, $d_\sigma = -0.3$ meV considering a coupling $J_1 = 1 \times 10^{-2}$ meV and $J_2 = 1.4 \times 10^{-2}$ meV. Initial state is $|\psi_0\rangle = \sum_{\mu_1\mu_2} |\mu_1, m_\sigma = -1, \mu_2\rangle/d$ (where $d = 4$ is the qudit dimension). (c) Controlled-phase gate error as a function of the maximum driving field amplitude B_1: best working spot at $B_1 = 20$ G.

situation can be easily achieved by considering a switch with spin larger than $1/2$ and then only focusing on the effective doublet formed by two of its energy levels. For instance, we consider here a Ni^{2+} ion (spin 1) with a typical axial zero-field splitting $d_\sigma = -0.3$ meV and g factor $g_\sigma = 2.2$. In an external field of ~ 1 T parallel to the easy axis, the gap between $m_\sigma = -1$ and $m_\sigma = 0$ is very different from that between $m_\sigma = 0$ and $m_\sigma = 1$. Hence, we can neglect $m_\sigma = 1$ states and use $|m_\sigma = -1, 0\rangle$ as an effective two-level switch, with $\Delta = d_\sigma - g_\sigma \mu_B B_0$. A sizable d_σ is important to ensure factorization between qudit and switch states, by making the

coupling J_i significantly smaller than the difference between switch and qudit energy gaps.

We now illustrate how to obtain an effectively switchable qudit-qudit coupling in the presence of permanent qudit-switch interactions, which cannot be tuned *in situ*. In the above conditions and by keeping the state of the switch frozen to $m_\sigma = -1$, in the idle phase the state of the two qudits remains decoupled; i.e., the "always-on" J_i interactions with the central σ merely renormalize their Zeeman energies. To turn the effective qudit-qudit coupling on, we apply a 2π excitation pulse to the switch, depending on the state of both qudits, as depicted by arrows in Fig. 6(a). Here we report the level diagram of the two-qudit **S**1 system (but the situation is analogous for **C**1), with different colors indicating different states of the switch. In particular, black levels refer to states with $m_\sigma = -1$ (corresponding to the idle phase with the switch open; see inset), while purple ones are characterized by $m_\sigma = 0$ (switch closed). What turns the switch on are the conditional excitations of the switch [arrows in Fig. 6(a)], made possible by the interaction terms in $\mathcal{H}_{i-\sigma}$ in Eq. (15). These make the transition energies of the switch $\delta(\mu_1, \mu_2)$ dependent on the state of both qudits. In the case of **S** this can be easily computed to first order, finding

$$\delta(m_1, m_2) = g_s \mu_B B_0 + J_1 m_1 + J_2 m_2, \quad (16)$$

with $m_{1,2}$ the eigenvalues of $S_{1,2}^z$. Hence, all the gaps are distinguishable, provided that $J_{1,2}$ are significantly larger than the frequency broadening of the employed pulses [78]. Such a broadening strongly depends on the shape of the pulses used to control the system. Again, the use of proper pulse shaping [66–74] or optimal quantum control techniques [75] could significantly reduce leakage, while keeping the duration of the pulses relatively short. However, a deep study of leakage should be addressed in a separate work, with a real system at hand. Here we only note that larger values of J_i allow us to employ larger B_1 and hence to implement faster two-qudit gates, which are therefore less subject to decoherence. Hence, we have used rather large J_i, leading to two-qudit gates lasting less than 25 ns. Then, we have optimized B_1 to get the lowest error (see below).

A resonant 2π pulse as illustrated above adds a π phase to the addressed component of the two-qudit wave function. By properly detuning the pulse from the energy gaps of Eq. (16) (i.e., implementing a semiresonant transition [79]), an arbitrary phase can be added. Provided all transitions are resolved ($J_1 \neq J_2$), this scheme can be used to add a specific phase to all the different two-qudit states, thus implementing the most general qudit-qudit controlled-phase gate. All in all, the presence of a magnetic switch makes it possible to transform a permanent interaction into a switchable one [2,5].

We implement this scheme on a pair of $S = 3/2$ Cr^{3+} qudits with $B_0 = 1$ T and on two real Cu_3 triangles, linked via a Ni^{2+} ion and rotated relative to each other to make them inequivalent through their intrinsic anisotropy Fig. 7(a). Results for **S** and **C** are shown in Figs. 6(b) and 7(b), together with the detailed list of parameters. We initialize the system in the state $|\psi_0\rangle = \sum_{\mu_1 \mu_2} |\mu_1, m_\sigma = -1, \mu_2\rangle / d$, i.e., a uniform superposition of all the d^2 components two-qudits states, in the subspace with the state of the switch frozen in $m_\sigma = -1$.

Analogously to single-qudit gates, this state is particularly error prone, since all its components (even those not evolving for the two-qudit gate) are present and hence subject to decoherence. The reported numerical simulations include the parallel pulses used to implement the desired phases and the effect of pure dephasing. Although in general a different phase can be added to each two-qudit state component, here we add phases to three components for clarity of presentation. We have performed several tests with different B_1 values as shown in Fig. 7(c), in order to find the best spot considering the effect of both leakage (increasing with B_1) and decoherence (increasing with the gate duration and hence decreasing with B_1). We find that $B_1 = 20$ G as the optimal driving field amplitude for both **S** and **C** cases. At fixed B_1, the duration of the pulse is proportional to the two-qudit phase we aim to add [79]. Here, however, since we are implementing three gates (with different phases) in parallel, we have properly rescaled B_1 in order to fix the same duration for all three simultaneous pulses (using $B_1 = 20$ G as maximum amplitude). Finally, we choose $T_2 = 3$ μs for the two qudits and 1 μs for the switch, a reasonable choice for a Ni complex [80].

Even for this small d and rather short gate duration, we find a remarkable advantage in using **C** compared to **S**, thanks to the suppression of decoherence in the latter. Indeed, using the same B_1 (and hence roughly the same gate duration), the error is reduced from 4.2% in **S** to 1.7% in **C**. This is remarkably good considering that we have used realistic parameters for the qudits and Ni^{2+} ions, as well as for the qudit-switch interaction. By comparing Figs. 6(b) and 7(b), we note that **C** still shows a significantly larger leakage error (secondary oscillations), which could be further reduced by proper pulse engineering or by increasing $J_{1,2}$ (and hence the spectral separation between the switch excitations) via proper synthesis. Finally, results could be improved also by extending the switch coherence.

VI. DISCUSSION AND CONCLUSIONS

To summarize, we have shown how to exploit molecular nanomagnets as optimal qudits for implementing a universal set of one- and two-qudit gates. The possibility offered by chemistry to synthesize complex multispin clusters with tailored interactions enables one to design efficient schemes to decompose general qudit operations. In particular, multispin molecules with competing exchange interactions are characterized by several low-energy multiplets with strongly suppressed decoherence, compared to the simpler case of single-ion spin-S qudits [39]. In addition, typical anisotropic and/or low-symmetry terms introduce dipole matrix elements between most of them, thus significantly reducing the number of consecutive pulses needed to implement a given unitary. By exploiting both of these features, we have demonstrated by realistic numerical simulations good fidelities in the implementation of paradigmatic gates (such as the Hadamard gate on a qudit, analogous to the multiqubit quantum Fourier transform). This makes properly engineered molecular nanomagnets competitive with other qudit platforms [23,24] and with more advanced qubit architectures [81,82].

It is also worth mentioning that the use of a (multi)qudit encoding to realize universal quantum computation protocols

offers intrinsic advantages over the corresponding multiqubit version for an equivalent total dimension of the computational space. Indeed, in addition to asymptotic logarithmic improvements in the total gate count for a generic unitary decomposition [54], qudit-based logic can reduce the number of required two-body operations. This is well exemplified by the realization of the QFT algorithm via H_d presented in this work, and is particularly relevant for near-term quantum computing platforms, where connectivity between computational units is often limited in practice and two-body operations are notably slower and more error prone compared to single-body ones.

APPENDIX A: DERIVATION OF THE MASTER EQUATION

We outline here a brief derivation of the master equation used to describe the incoherent dynamics of the system, driven at low temperature by the interaction with the nuclear spin bath. The system-bath Hamiltonian $\mathcal{H}_{SB}$ is given by

$$\mathcal{H}_{SB} = \sum_{j=1}^{N} \sum_{n=1}^{M} \sum_{\alpha,\beta=x,y,z} d_{jn}^{\alpha\beta} s_j^{\alpha} \otimes I_n^{\beta}, \tag{A1}$$

where N is the number of magnetic ions in the system and M the number of nuclear spins in the bath, I_n^{β} are bath spin operators, and $d_{jn}^{\alpha\beta}$ are dipolar couplings defined in the text. By moving to the interaction picture with respect to the Hamiltonians of the free system, $\mathcal{H}_S$, and of the bath, $\mathcal{H}_B$, we get

$$\mathcal{H}_{SB}(t) = e^{i(\mathcal{H}_S + \mathcal{H}_B)t} \mathcal{H}_{SB} e^{-i(\mathcal{H}_S + \mathcal{H}_B)t}$$

$$= \sum_{n=1}^{M} \sum_{\mu\nu} \sum_{\beta} L_{n,\mu\nu}^{\beta} e^{i(E_\mu - E_\nu)t} |\mu\rangle\langle\nu| \otimes I_n^{\beta}(t). \tag{A2}$$

Here, $|\mu\rangle$ is the basis of the system eigenstates, $\mathcal{H}_S = \sum_\mu E_\mu |\mu\rangle\langle\mu|$, we have indicated by $I_n^{\beta}(t) = e^{i\mathcal{H}_B t} I_n^{\beta} e^{-i\mathcal{H}_B t}$ the nuclear spin operators in the interaction picture, and we have introduced

$$L_{n,\mu\nu}^{\beta} = \sum_{j=1}^{N} \sum_{\alpha=x,y,z} d_{jn}^{\alpha\beta} \langle\mu|s_j^{\alpha}|\nu\rangle, \tag{A3}$$

which contains the structure of the system eigenstates in the matrix elements $\langle\mu|s_j^{\alpha}|\nu\rangle$. Then, in the Born and Markov approximations, the dynamics of the system is described by the master equation [83]

$$\dot{\rho}(t) = -\int_0^\infty dt' \mathrm{tr}_B[\mathcal{H}_{SB}(t), [\mathcal{H}_{SB}(t - t'), \rho(t) \otimes \rho_B]], \tag{A4}$$

where $\rho(t) = \mathrm{tr}_B[\rho_{SB}(t)]$ is the reduced density matrix of the system. By substituting Eq. (A2) into Eq. (A4) and taking the

secular approximation, we obtain

$$\dot{\rho}(t) = -\sum_{n,n'=1}^{M} \sum_{\mu,\nu} \sum_{\beta\beta'} \left\{ L_{n,\mu\mu}^{\beta} L_{n',\nu\nu}^{\beta',*} \zeta_{nn'}^{\beta\beta'}(\omega) \right.$$

$$\left. \times [|\mu\rangle\langle\mu|\nu\rangle\langle\nu|\rho(t) - |\mu\rangle\langle\mu|\rho(t)|\nu\rangle\langle\nu|] + \mathrm{H.c.} \right\}, \tag{A5}$$

where we have introduced the bath spectral functions

$$\zeta_{nn'}^{\beta\beta'}(\omega) = \int_0^\infty dt \, \mathrm{tr}_B[I_n^{\beta}(t) I_{n'}^{\beta'}(0)\rho_B] e^{i\omega t}. \tag{A6}$$

Within the secular approximation, in Eq. (A5) we have neglected fast oscillating terms and in particular jump operators of the form $|\mu\rangle\langle\nu|$ (with $\mu \neq \nu$) which are ineffective, because the difference between $\Delta_{\mu\nu}$ and the bath energy gaps is much larger than the system-bath interaction. In this limit, no relaxation is induced on the system by its coupling with the environment and only diagonal operators $|\mu\rangle\langle\mu|$ are retained, leading to pure dephasing.

For a bath of interacting spins, the bath spectral functions $\zeta_{nn'}^{\beta\beta'}$ are in general unknown. Their computation from first principles requires advanced numerical methods, such as the cluster correlation expansion [28,84,85], and is beyond the scope of the present work.

By rearranging terms in Eq. (A5), we obtain the final form of the master equation reported in the main text:

$$\dot{\rho}(t) = -i[\mathcal{H}_{LS}, \rho(t)] + \sum_{\mu\nu} \Gamma_{\mu\nu}[2|\mu\rangle\langle\mu|\rho(t)|\nu\rangle\langle\nu|$$

$$- |\mu\rangle\langle\mu|\delta_{\mu\nu}\rho(t) - \rho(t)|\nu\rangle\langle\nu|\delta_{\mu\nu}], \tag{A7}$$

where we have introduced the rates

$$\Gamma_{\mu\nu} = \sum_{n,n'=1}^{M} \sum_{\beta,\beta'} L_{n,\mu\mu}^{\beta} L_{n',\nu\nu}^{\beta',*} \chi_{nn'}^{\alpha\alpha'}(0), \tag{A8}$$

with

$$\chi_{nn'}^{\alpha\alpha'}(0) = \frac{1}{2} \int_{-\infty}^{\infty} dt \, \mathrm{tr}_B[I_n^{\alpha}(t) I_{n'}^{\alpha'}(0)\rho_B]. \tag{A9}$$

The Lamb shift Hamiltonian $\mathcal{H}_{LS} = \sum_\mu S_\mu |\mu\rangle\langle\mu|$ only describes a small renormalization of the system energies due to the coupling with the bath, and we therefore neglect it in the simulations.

APPENDIX B: ALGORITHM FOR DECOMPOSITION IN PLANAR ROTATIONS

An iterative procedure to decompose an arbitrary $W \in SU(d)$ in planar rotations is the following. First, we multiply W on the right-hand side by $U_{d-1\,d}(\theta_{\frac{d(d-1)}{2}}, \beta_{\frac{d(d-1)}{2}})$, with $\theta_{\frac{d(d-1)}{2}}$ and $\beta_{\frac{d(d-1)}{2}}$ such that the $(d, d-1)$ element of the resulting $W_1 = WU_{d-1,d}(\theta_{\frac{d(d-1)}{2}}, \beta_{\frac{d(d-1)}{2}})$ is zero. Next, we compute $W_2 = W_1 U_{d-2,d}(\theta_{\frac{d(d-1)}{2}-1}, \beta_{\frac{d(d-1)}{2}-1})$ fixing, as before, $\theta_{\frac{d(d-1)}{2}-1}$ and $\beta_{\frac{d(d-1)}{2}-1}$ angles to nullify the $W_2(d, d-2)$ element. Proceeding in this way, we obtain the W_{d-1} matrix that has all

TABLE I. Parameters to decompose the H_4 gate into PRs (keeping three significant digits).

μ, ν	$\theta/2$	β	α
3,4	$-\pi/4$	$\pi/2$	
2,4	$\arctan(1/\sqrt{2})$	0	
1,4	$\arctan(1/\sqrt{3})$	$\pi/2$	
2,3	0.912	-0.464	
1,3	$\arctan(-1/\sqrt{2})$	$-\pi/4$	
1,2	$\pi/4$	$\pi/4$	
3,4			$\pi/8$
1,2			$3\pi/8$

zero in the d column and a row apart for the (d, d)th element which must have magnitude 1 because the matrix is unitary. Without affecting the dth column and row, the same scheme could be repeated for all the other lines. The resulting matrix will be a diagonal one:

$$WU_{d-1,d}U_{d-2,d}\ldots U_{1,d}U_{d-2,d-1}\ldots U_{1,3}U_{1,2}$$
$$= \Lambda(e^{i\alpha_1}, e^{i\alpha_2}, \ldots, e^{i\alpha_{d-1}}, e^{-i\sum_{k=1}^{d-1}\alpha_k}), \quad (B1)$$

where Λ is a diagonal matrix with the elements shown in brackets. By reverting this equation we obtain the decomposition of W in $\frac{d(d-1)}{2}$ PRs.

The sequence of pulses to implement H_4, H_6, and H_8 by decomposing it into PRs is reported in Tables I–III, where full connectivity between the levels is assumed, and where parameters θ and β are the $U_{\mu\nu}$ rotation pulse parameters [Eq. (8)]; α is the $P_{\mu\nu}$ phase pulse parameter [Eq. (10)]. The full sequence of pulses in the case of linear connectivity for H_4 is given by Eq. (B2), resulting in 14 pulses; for H_6 it is

TABLE II. Parameters to decompose the H_6 gate into PRs (keeping three significant digits).

μ, ν	$\theta/2$	β	α
5,6	$\pi/4$	$-2\pi/3$	
4,6	$\arctan(1/\sqrt{2})$	$-\pi/3$	
3,6	$\pi/6$	2π	
2,6	$\arctan(1/2)$	$\pi/3$	
1,6	$\arctan(1/\sqrt{5})$	$2\pi/3$	
4,5	$\text{arccot}(\sqrt{3/7})$	$-\arctan(3\sqrt{3})$	
3,5	$\text{arccot}(2\sqrt{5/19})$	$\text{arccot}(4/\sqrt{3})$	
2,5	$\arctan(\sqrt{31/65})$	$\pi - \arctan(5\sqrt{3}/7)$	
1,5	$\arctan(1/2)$	$-2\pi/3$	
3,4	$\arctan(\sqrt{37/13})$	$-\arctan(2\sqrt{3}/5)$	
2,4	$\text{arccot}(2\sqrt{5/19})$	$1/2(\pi + \arctan(8\sqrt{3}/13))$	
1,4	$\pi/6$	$-\pi/2$	
2,3	$\arctan(\sqrt{7/3})$	$\arctan(1/3\sqrt{3})$	
1,3	$\arctan(1/\sqrt{2})$	$-5\pi/6$	
1,2	$\pi/4$	1.047	
5,6			$-\pi/3$
3,4			$\pi/2$
2,3			$2\pi/3$

TABLE III. Parameters to decompose H_8 gate into PRs (keeping three significant digits).

μ, ν	$\theta/2$	β	α
7,8	$\pi/4$	$-3\pi/4$	
6,8	$\arctan(1/\sqrt{2})$	$-\pi/2$	
5,8	$\pi/6$	$-\pi/4$	
4,8	$2\arctan(1/2)$	0	
3,8	$\arctan(1/\sqrt{5})$	$\pi/4$	
2,8	$\text{arccot}(\sqrt{6})$	$\pi/2$	
1,8	$\arctan(1/\sqrt{7})$	$3\pi/4$	
6,7	1.016	4.457	
5,7	0.824	-0.5	
4,7	0.687	0.843	
3,7	0.573	2.213	
2,7	0.474	-2.657	
1,7	0.388	-1.178	
5,6	1.093	-1.249	
4,6	0.895	0.655	
3,6	0.731	2.585	
2,6	0.573	-1.714	
1,6	0.421	0.393	
4,5	1.113	-0.663	
3,5	0.895	1.834	
2,5	0.687	-1.906	
1,5	0.464	0.785	
3,4	1.093	-0.071	
2,4	0.824	3.034	
1,4	0.524	0	
2,3	1.016	0.530	
1,3	0.615	-1.963	
1,2	0.785	1.178	
7,8			$\pi/16$
6,7			π
5,6			$7\pi/16$
3,4			$11\pi/16$
1,2			$5\pi/16$

given by Eq. (B3), resulting in 38 pulses; and lastly, for H_8 it is given by Eq. (B4), resulting in 75 pulses. The $\pi_{\mu\nu}^{\pm}$ pulses are properly used to swap the levels in order to perform U rotations on adjacent μ, ν levels:

$$H_4 = P_{1,2}P_{3,4}$$
$$\times U_{1,2}$$
$$\times \pi_{1,2}^{+}U_{1,3}\pi_{1,2}^{-}U_{2,3}$$
$$\times \pi_{3,4}^{+}\pi_{2,3}^{+}U_{1,4}\pi_{2,3}^{-}U_{2,4}\pi_{3,4}^{-}U_{3,4}, \quad (B2)$$

$$H_6 = P_{5,6}P_{3,4}P_{2,3}$$
$$\times U_{1,2}$$
$$\times \pi_{2,3}^{+}U_{1,3}\pi_{2,3}^{-}U_{2,3}$$
$$\times \pi_{3,4}^{+}\pi_{2,3}^{+}U_{1,4}\pi_{2,3}^{-}U_{2,4}\pi_{3,4}^{-}U_{3,4}$$
$$\times \pi_{4,5}^{+}\pi_{3,4}^{+}\pi_{2,3}^{+}U_{1,5}\pi_{2,3}^{-}U_{2,5}\pi_{3,4}^{-}U_{3,5}\pi_{4,5}^{-}U_{4,5}$$
$$\times \pi_{5,6}^{+}\pi_{4,5}^{+}\pi_{3,4}^{+}\pi_{2,3}^{+}U_{1,6}\pi_{2,3}^{-}U_{2,6}\pi_{3,4}^{-}U_{3,6}\pi_{4,5}^{-}U_{4,6}\pi_{5,6}^{-}U_{5,6}, \quad (B3)$$

TABLE IV. Parameters to decompose the H_d gate into QHRs (keeping three significant digits).

H_3	v_i	ϕ_i
1	$\frac{1}{2}\sqrt{1+\frac{1}{\sqrt{3}}}[1-\sqrt{3}, 1, 1]^T$	π
2	$\frac{1}{\sqrt{2}}[0, 1, -1]^T$	$\pi/2$
H_4		
1	$\frac{1}{2}[-1, 1, 1, 1]^T$	π
2	$\frac{1}{\sqrt{2}}[0, 1, 0, -1]^T$	$\pi/2$
H_6		
1	$[0.544i, -0.375i, -0.375i, -0.375i, -0.375i, -0.375i]^T$	$-\pi$
2	$[0, 0.575 + 0.220i, 0.244 - 0.261i, 0.071 + 0.103i, -0.331 + 0.135i, -0.559 - 0.197i]^T$	1.937
3	$[0, 0, -0.490 + 0.626i, 0.113 - 0.466i, 0.352 - 0.055i, 0.025 - 0.105i]^T$	-2.478
4	$[0, 0, 0, -0.322 + 0.537i, 0.395 - 0.657i, -0.073 + 0.121i]^T$	-2.601
H_8		
1	$[0.569i, -0.311i, -0.311i, -0.311i, -0.311i, -0.311i, -0.311i]^T$	$-\pi$
2	$[0, 0.432 + 0.384i, 0.230 - 0.305i, 0.238 - 0.048i, 0.062 + 0.139i, -0.194 + 0.146i, -0.381 - 0.030i, -0.388 - 0.286i]^T$	2.297
3	$[0, 0, 0.174 + 0.819i, -0.228 + 0.008i, -0.097 - 0.316i, 0.159 - 0.231i, 0.060 - 0.056i, -0.067 - 0.22i]^T$	2.932
4	$[0, 0, 0, 0.233 + 0.568i, -0.146 + 0.133i, -0.336 - 0.475i, 0.352 - 0.320i, -0.103 + 0.094i]^T$	2.752
5	$[0, 0, 0, 0, 0.046 + 0.355i, 0.032 + 0.251i, -0.110 - 0.856i, 0.032 + 0.251i]^T$	3.014

$$H_8 = P_{7,8}P_{6,7}P_{5,6}P_{3,4}P_{1,2}$$
$$\times U_{1,2}$$
$$\times \pi_{2,3}^+ U_{1,3}\pi_{2,3}^- U_{2,3}$$
$$\times \pi_{3,4}^+\pi_{2,3}^+ U_{1,4}\pi_{2,3}^- U_{2,4}\pi_{3,4}^- U_{3,4}$$
$$\times \pi_{4,5}^+\pi_{3,4}^+\pi_{2,3}^+ U_{1,5}\pi_{2,3}^- U_{2,5}\pi_{3,4}^- U_{3,5}\pi_{4,5}^- U_{4,5}$$
$$\times \pi_{5,6}^+\pi_{4,5}^+\pi_{3,4}^+\pi_{2,3}^+ U_{1,6}\pi_{2,3}^- U_{2,6}\pi_{3,4}^- U_{3,6}\pi_{4,5}^- U_{4,6}\pi_{5,6}^- U_{5,6}$$
$$\times \pi_{6,7}^+\pi_{5,6}^+\pi_{4,5}^+\pi_{3,4}^+\pi_{2,3}^+ U_{1,7}\pi_{2,3}^- U_{2,7}\pi_{3,4}^- U_{3,7}\pi_{4,5}^- U_{4,7}$$
$$\times \pi_{5,6}^- U_{5,7}\pi_{6,7}^- U_{6,7}$$
$$\times \pi_{7,8}^+\pi_{6,7}^+\pi_{5,6}^+\pi_{4,5}^+\pi_{3,4}^+\pi_{2,3}^+ U_{1,8}\pi_{2,3}^- U_{2,8}\pi_{3,4}^- U_{3,8}$$
$$\times \pi_{4,5}^- U_{4,8}\pi_{5,6}^- U_{5,8}\pi_{6,7}^- U_{6,8}\pi_{7,8}^- U_{7,8}. \qquad \text{(B4)}$$

APPENDIX C: ALGORITHM FOR DECOMPOSITION IN QUANTUM HOUSEHOLDER REFLECTIONS

Equation (12) shows the sequence of QHRs needed to decompose an arbitrary $W \in SU(d)$. All the v_i vectors and ϕ_i phases can be easily determined through an iterative procedure. Given the target matrix W, the parameters of the first QHR $M_1 = M(v_1, \phi_1)$ are defined as

$$\phi_1 = 2 \arg(1 - w_{11}) - \pi,$$
$$v_1 = \frac{1}{e^{-i\phi_1} - 1}\sqrt{\frac{2 \sin(\phi_1/2)}{|1 - w_{11}|}}(|w_1\rangle - |e_1\rangle), \qquad \text{(C1)}$$

where w_1 is the first column of the W matrix, w_{11} is the first element of the w_1 vector, and $|e_1\rangle = [1, 0, \ldots, 0]^T$. To proceed, we apply $M(w_1, -\phi_1)$ on the left-hand side of the initial matrix, defining a new matrix which we call $W_1 = M(w_1, -\phi_1)W$. This latter is characterized by having all null elements on the first row and the first column except for the diagonal one, which will be 1. Restarting from W_1 and defining w_2, ϕ_2, and $|e_2\rangle$ analogously as done for w_1, ϕ_1, and $|e_1\rangle$, we find the parameters for M_2. Applying this procedure d times, all the v_i vectors and ϕ_i phases are determined. In Table IV we report all the parameters to decompose H$_4$, H$_6$, and H$_8$.

[1] A. J. Heinrich, W. D. Oliver, L. M. K. Vandersypen, A. Ardavan, R. Sessoli, D. Loss, A. Bleszynski Jayich, J. Fernandez-Rossier, A. Laucht, and A. Morello, Quantum-coherent nanoscience, Nat. Nanotechnol. **16**, 1318 (2021).

[2] A. Chiesa, G. F. S. Whitehead, S. Carretta, L. Carthy, G. A. Timco, S. J. Teat, G. Amoretti, E. Pavarini, R. E. P. Winpenny, and P. Santini, Molecular nanomagnets with switchable coupling for quantum simulation, Sci. Rep. **4**, 7423 (2015).

[3] D. Aguilà, D. Barrios, V. Velasco, O. Roubeau, A. Repollés, P. Alonso, J. Sesé, S. Teat, F. Luis, and G. Aromí, Heterodimetallic [LnLn′] lanthanide complexes: Toward a chemical design of two-qubit molecular spin quantum gates, J. Am. Chem. Soc. **136**, 14215 (2014).

[4] A. Ardavan, A. M. Bowen, A. Fernandez, A. J. Fielding, D. Kaminski, F. Moro, C. A. Muryn, M. D.Wise, A. Ruggi, E. J. L. McInnes, K. Severin, G. A. Timco, C. R. Timmel, F. Tuna, G. F. S. Whitehead, and R. E. P. Winpenny, Engineering coherent interactions in molecular nanomagnet dimers, npj Quantum Inf. **1**, 15012 (2015).

[5] J. Ferrando-Soria, E. Moreno-Pineda, A. Chiesa, A. Fernandez, S. A. Magee, S. Carretta, P. Santini, I. Vitorica-Yrezabal, F. Tuna, E. J. L. McInness, and R. E. P. Winpenny, A modular design of molecular qubits to implement universal quantum gates, Nat. Commun. **7**, 11377 (2016).

[6] M. Atzori, L. Tesi, E. Morra, M. Chiesa, L. Sorace, and R. Sessoli, Room-temperature quantum coherence and Rabi oscillations in vanadyl phthalocyanine: Toward multifunctional molecular spin qubits, J. Am. Chem. Soc. **138**, 2154 (2016).

[7] M. Atzori, E. Morra, L. Tesi, A. Albino, M. Chiesa, L. Sorace, and R. Sessoli, Quantum coherence times enhancement in

vanadium(IV)-based potential molecular qubits: The key role of the vanadyl moiety, J. Am. Chem. Soc. **138**, 11234 (2016).

[8] E. Macaluso, M. Rubín, D. Aguilà, A. Chiesa, J. I. M. L. A. Barrios, P. J. Alonso, O. Roubeau, F. Luis, G. Aromí, and S. Carretta, A heterometallic [LnLn′Ln] lanthanide complex as a qubit with embedded quantum error correction, Chem. Sci. **11**, 10337 (2020).

[9] A. Gaita-Ariño, F. Luis, S. Hill, and E. Coronado, Molecular spins for quantum computation, Nat. Chem. **11**, 301 (2019).

[10] M. Atzori and R. Sessoli, The second quantum revolution: Role and challenges of molecular chemistry, J. Am. Chem. Soc. **141**, 11339 (2019).

[11] C. Bonizzoni, A. Ghirri, F. Santanni, M. Atzori, L. Sorace, R. Sessoli, and M. Affronte, Storage and retrieval of microwave pulses with molecular spin ensembles, npj Quantum Inf. **6**, 68 (2020).

[12] S. J. Lockyer, A. Chiesa, G. A. Timco, E. J. L. McInnes, T. S. Bennett, I. J. Vitorica-Yrezebal, S. Carretta, and R. E. P. Winpenny, Targeting molecular quantum memory with embedded error correction, Chem. Sci. **12**, 9104 (2021).

[13] S. Carretta, D. Zueco, A. Chiesa, A. Gómez-León, and F. Luis, A perspective on scaling up quantum computation with molecular spins, Appl. Phys. Lett. **118**, 240501 (2021).

[14] J. Liu, J. Mrozek, A. Ullah, Y. Duan, J. J. Baldoví, E. Coronado, A. Gaita-Ariño, and A. Ardavan, Quantum coherent spin-electric control in a molecular nanomagnet at clock transitions, Nat. Phys. **17**, 1205 (2021).

[15] Y. Bae, K. Yang, P. Willke, T. Choi, A. Heinrich, and C. Lutz, Enhanced quantum coherence in exchange coupled spins via singlet-triplet transitions, Sci. Adv. **4**, eaau4159 (2018).

[16] P. Vorndamme and J. Schnack, Decoherence of a singlet-triplet superposition state under dipolar interactions of an uncorrelated environment, Phys. Rev. B **101**, 075101 (2020).

[17] I. Gimeno, W. Kersten, M. Pallarés, P. Hermosilla, M. Martínez-Pérez, M. Jenkins, A. Angerer, C. Sánchez-Azqueta, D. Zueco, J. Majer, A. Lostao, and F. Luis, Enhanced molecular spin-photon coupling at superconducting nanoconstrictions, ACS Nano **14**, 8707 (2020).

[18] R. Hussain, G. Allodi, A. Chiesa, E. Garlatti, D. Mitcov, A. Konstantatos, K. Pedersen, R. D. Renzi, S. Piligkos, and S. Carretta, Coherent manipulation of a molecular Ln-based nuclear qudit coupled to an electron qubit, J. Am. Chem. Soc. **140**, 9814 (2018).

[19] S. Chicco, A. Chiesa, G. Allodi, E. Garlatti, M. Atzori, L. Sorace, R. De Renzi, R. Sessoli, and S. Carretta, Controlled coherent dynamics of [VO(TPP)], a prototype molecular nuclear qudit with an electronic ancilla, Chem. Sci. **12**, 12046 (2021).

[20] C. Godfrin, A. Ferhat, R. Ballou, S. Klyatskaya, M. Ruben, W. Wernsdorfer, and F. Balestro, Operating Quantum States in Single Magnetic Molecules: Implementation of Grover's Quantum Algorithm, Phys. Rev. Lett. **119**, 187702 (2017).

[21] E. Moreno-Pineda, C. Godfrin, F. Balestro, W. Wernsdorfer, and M. Ruben, Molecular spin qudits for quantum algorithms, Chem. Soc. Rev. **47**, 501 (2018).

[22] Y. Wang, Z. Hu, B. C. Sanders, and S. Kais, Qudits and high-dimensional quantum computing, Front. Phys. **8**, 479 (2020).

[23] M. Ringbauer, M. Meth, L. Postler, R. Stricker, R. Blatt, P. Schindler, and T. Monz, A universal qudit quantum processor with trapped ions, Nat. Phys. **18**, 1053 (2022).

[24] Y. Chi, J. Huang, Z. Zhang, J. Mao, Z. Zhou, X. Chen, C. Zhai, J. Bao, T. Dai, H. Yuan, M. Zhang, D. Dai, B. Tang, Y. Yang, Z. Li, Y. Ding, L. K. Oxenløwe, M. G. Thompson, J. L. O'Brien, Y. Li *et al.*, A programmable qudit-based quantum processor, Nat. Commun. **13**, 1166 (2022).

[25] F. Tacchino, A. Chiesa, R. Sessoli, I. Tavernelli, and S. Carretta, A proposal for using molecular spin qudits as quantum simulators of light-matter interactions, J. Mater. Chem. C **9**, 10266 (2021).

[26] D. González-Cuadra, T. V. Zache, J. Carrasco, B. Kraus, and P. Zoller, Hardware efficient quantum simulation of non-Abelian gauge theories with qudits on Rydberg platforms, Phys. Rev. Lett. **129**, 160501 (2022).

[27] A. Chiesa, E. Macaluso, F. Petiziol, S. Wimberger, P. Santini, and S. Carretta, Molecular nanomagnets as qubits with embedded quantum-error correction, J. Phys. Chem. Lett. **11**, 8610 (2020).

[28] F. Petiziol, A. Chiesa, S. Wimberger, P. Santini, and S. Carretta, Counteracting dephasing in molecular nanomagnets by optimized qudit encodings, npj Quantum Inf. **7**, 133 (2021).

[29] L. M. Baker *et al.*, Studies of a large odd-numbered odd-electron metal ring: Inelastic neutron scattering and muon spin relaxation spectroscopy of Cr$_8$Mn, Chem. Eur. J. **22**, 1779 (2016).

[30] R. J. Woolfson, G. A. Timco, A. Chiesa, I. J. Vitorica-Yrezabal, F. Tuna, T. Guidi, E. Pavarini, P. Santini, S. Carretta, and R. E. P. Winpenny, [CrF(O$_2$C^{t}Bu)$_2$]$_9$: Synthesis and characterization of a regular homometallic ring with an odd number of metal centers and electrons, Angew. Chem. Int. Ed. **55**, 8856 (2016).

[31] A. Ghirri, A. Chiesa, S. Carretta, F. Troiani, J. van Tol, S. Hill, I. Vitorica-Yrezabal, G. A. Timco, R. E. P. Winpenny, and M. Affronte, Coherent spin dynamics in molecular Cr$_8$Zn wheels, J. Phys. Chem. Lett. **6**, 5062 (2015).

[32] F. Adelnia, A. Chiesa, S. Bordignon, S. Carretta, A. Ghirri, A. Candini, C. Cervetti, M. Evangelisti, M. Affronte, I. Sheikin, R. Winpenny, G. Timco, F. Borsa, and A. Lascialfari, Low temperature magnetic properties and spin dynamics in single crystals of Cr$_8$Zn antiferromagnetic molecular rings, J. Chem. Phys. **143**, 244321 (2015).

[33] J. Schnack, Effects of frustration on magnetic molecules: A survey from Olivier Kahn until today, Dalton Trans. **39**, 4677 (2010).

[34] E. Garlatti, S. Carretta, P. Santini, G. Amoretti, M. Mariani, A. Lascialfari, S. Sanna, K. Mason, J. Chang, P. Tasker, and E. K. Brechin, Relaxation dynamics in a Fe$_7$ nanomagnet, Phys. Rev. B **87**, 054409 (2013).

[35] J. van Slageren, P. Rosa, A. Caneschi, R. Sessoli, H. Casellas, Y. V. Rakitin, L. Cianchi, F. Del Giallo, G. Spina, A. Bino, A.-L. Barra, T. Guidi, S. Carretta, and R. Caciuffo, Static and dynamic magnetic properties of an [Fe$_{13}$] cluster, Phys. Rev. B **73**, 014422 (2006).

[36] M. Antkowiak, P. Kozłowski, G. Kamieniarz, G. A. Timco, F. Tuna, and R. E. P. Winpenny, Detection of ground states in frustrated molecular rings by in-field local magnetization profiles, Phys. Rev. B **87**, 184430 (2013).

[37] W. Florek, M. Antkowiak, and G. Kamieniarz, Sequences of ground states and classification of frustration in odd-numbered antiferromagnetic rings, Phys. Rev. B **94**, 224421 (2016).

[38] M. Baker, G. Timco, S. Piligkos, J. Mathieson, H. Mutka, F. Tuna, P. Kozlowski, M. Antkowiak, T. Guidi, T. Gupta, H. Rath, R. Woolfson, G. Kamieniarz, R. Pritchard, H. Weihe, L. Cronin, G. Rajaraman, D. Collison, E. McInnes, and R. Winpenny, A classification of spin frustration in molecular magnets from a physical study of large odd-numbered-metal, odd electron rings, Proc. Natl. Acad. Sci. USA **109**, 19113 (2012).

[39] A. Chiesa, F. Petiziol, M. Chizzini, P. Santini, and S. Carretta, Theoretical design of optimal molecular qudits for quantum error correction, J. Phys. Chem. Lett. **13**, 6468 (2022).

[40] K.-Y. Choi, Y. H. Matsuda, H. Nojiri, U. Kortz, F. Hussain, A. C. Stowe, C. Ramsey, and N. S. Dalal, Observation of a Half Step Magnetization in the Cu_3-Type Triangular Spin Ring, Phys. Rev. Lett. **96**, 107202 (2006).

[41] E. Garlatti, S. Carretta, M. Affronte, E. C. Sanudo, G. Amoretti, and P. Santini, Magnetic properties and relaxation dynamics of a frustrated Ni_7 molecular nanomagnet, J. Phys.: Condens. Matter **24**, 104006 (2012).

[42] T. Glaser, M. Heidemeier, T. Weyhermüller, R.-D. Hoffmann, H. Rupp, and P. Müller, Property-oriented rational design of single-molecule magnets: A C_3-symmetric Mn_6Cr complex based on three molecular building blocks with a spin ground state of S_t=21/2, Angew. Chem. Int. Ed. **45**, 6033 (2006).

[43] K. Vignesh, A. Soncini, S. Langley, W. Wernsdorfer, K. S. Murray, and G. Rajaraman, Ferrotoroidic ground state in a heterometallic $\{Cr^{III}Dy^{III}_6\}$ complex displaying slow magnetic relaxation, Nat. Commun. **8**, 1023 (2017).

[44] U. Kortz, N. K. Al-Kassem, M. G. Savelieff, N. A. Al Kadi, and M. Sadakane, Synthesis and characterization of copper-, zinc-, manganese-, and cobalt-substituted dimeric heteropolyanions, $[(\alpha\text{-}XW_9O_{33})_2M_3(H_2O)_3]^{n-}$ ($n = 12$, X = As^{III}, Sb^{III}, M = Cu^{2+}, Zn^{2+}; $n = 10$, X = Se^{IV}, Te^{IV}, M = Cu^{2+}) and $[(\alpha\text{-}AsW_9O_{33})_2WO(H_2O)M_2(H_2O)_2]^{10-}$ (M = Zn^{2+}, Mn^{2+}, Co^{2+}), Inorg. Chem. **40**, 4742 (2001).

[45] The spin Hamiltonian of **C**1 also includes a small axial anisotropic exchange contribution, not reported in the text but included in our simulations, according to Ref. [40].

[46] M. Fataftah, J. M. Zadrozny, S. C. Coste, M. J. Graham, D. M. Rogers, and D. E. Freedman, Employing forbidden transitions as qubits in a nuclear spin-free chromium complex., J. Am. Chem. Soc. **138**, 1344 (2016).

[47] Y.-S. Ding, Y.-F. Deng, and Y.-Z. Zheng, The rise of single-ion magnets as spin qubits, Magnetochemistry **2**, 40 (2016).

[48] K. Bader, M. Winkler, and J. van Slageren, Tuning of molecular qubits: Very long coherence and spin-lattice relaxation times, Chem. Commun. **52**, 3623 (2016).

[49] E. K. Brechin, S. G. Harris, S. Parsons, and R. E. P. Winpenny, Clusters from vertex- and face-sharing adamantane-like units: A new topology for multinuclear complexes, Angew. Chem. Int. Ed. Engl. **36**, 1967 (1997).

[50] The analysis can be easily extended to more complex situations.

[51] A. Abragam and B. Bleaney, *Electron Paramagnetic Resonance of Transition Ions* (Oxford University Press, Oxford, 1970).

[52] A. Caneschi, A. Dei, D. Gatteschi, C. A. Massa, L. A. Pardi, S. S. Poussereau, and L. Sorace, Evaluating the magnetic anisotropy in molecular rare earth compounds. gadolinium derivatives with semiquinone radical and diamagnetic analogues, Chem. Phys. Lett. **371**, 694 (2003).

[53] A. Bencini and D. Gatteschi, *EPR of Exchange Coupled Systems* (Springer-Verlag, Berlin, 1990).

[54] A. Muthukrishnan and C. R. Stroud, Multivalued logic gates for quantum computation, Phys. Rev. A **62**, 052309 (2000).

[55] S. G. Schirmer, A. D. Greentree, V. Ramakrishna, and H. Rabitz, Constructive control of quantum systems using factorization of unitary operators, J. Phys. A: Math. Gen. **35**, 8315 (2002).

[56] P. J. Low, B. M. White, A. A. Cox, M. L. Day, and C. Senko, Practical trapped-ion protocols for universal qudit-based quantum computing, Phys. Rev. Res. **2**, 033128 (2020).

[57] L. E. Fischer, D. Miller, F. Tacchino, P. K. Barkoutsos, D. J. Egger, and I. Tavernelli, Ancilla-free implementation of generalized measurements for qubits embedded in a qudit space, Phys. Rev. Res. **4**, 033027 (2022).

[58] D. D'Alessandro, *Introduction to Quantum Control and Dynamics* (CRC Press, Boca Raton, FL, 2007).

[59] More efficient decomposition techniques based on PRs are also known for linearly connected systems, which do not require additional π pulses nor explicit phase gates but still scale quadratically with d [56].

[60] P. A. Ivanov, E. S. Kyoseva, and N. V. Vitanov, Engineering of arbitrary U(N) transformations by quantum Householder reflections, Phys. Rev. A **74**, 022323 (2006).

[61] P. A. S. Cruickshank, D. R. Bolton, D. A. Robertson, R. I. Hunter, R. J. Wylde, and G. M. Smith, A kilowatt pulsed 94 GHz electron paramagnetic resonance spectrometer with high concentration sensitivity, high instantaneous bandwidth, and low dead time, Rev. Sci. Instrum. **80**, 103102 (2009).

[62] M. J. Graham, J. M. Zadrozny, M. Shiddiq, J. S. Anderson, M. S. Fataftah, S. Hill, and D. E. Freedman, Influence of electronic spin and spin-orbit coupling on decoherence in mononuclear transition metal complexes., J. Am. Chem. Soc. **136**, 7623 (2014).

[63] C. J. Wedge, G. A. Timco, E. T. Spielberg, R. E. George, F. Tuna, S. Rigby, E. J. L. McInnes, R. E. P. Winpenny, S. J. Blundell, and A. Ardavan, Chemical Engineering of Molecular Qubits, Phys. Rev. Lett. **108**, 107204 (2012).

[64] K. Bader, D. Dengler, S. Lenz, B. Endeward, S.-D. Jiang, P. Neugebauer, and J. van Slageren, Room temperature quantum coherence in a potential molecular qubit, Nat. Commun. **5**, 5304 (2014).

[65] J. M. Zadrozny, J. Niklas, O. G. Poluektov, and D. E. Freedman, Millisecond coherence time in a tunable molecular electronic spin qubit, ACS Cent. Sci. **1**, 488 (2015).

[66] J. M. Gambetta, F. Motzoi, S. T. Merkel, and F. K. Wilhelm, Analytic control methods for high-fidelity unitary operations in a weakly nonlinear oscillator, Phys. Rev. A **83**, 012308 (2011).

[67] F. Motzoi, J. M. Gambetta, P. Rebentrost, and F. K. Wilhelm, Simple Pulses for Elimination of Leakage in Weakly Nonlinear Qubits, Phys. Rev. Lett. **103**, 110501 (2009).

[68] M. Werninghaus, D. J. Egger, F. Roy, S. Machnes, F. K. Wilhelm, and S. Filipp, Leakage reduction in fast superconducting qubit gates via optimal control, npj Quantum Inf. **7**, 14 (2021).

[69] A. De, Fast two-quadrature adiabatic quantum gates for weakly nonlinear qubits: A tight-binding approach, Quantum Inf. Proc. **18**, 165 (2019).

[70] M. Chizzini, L. Crippa, L. Zaccardi, E. Macaluso, S. Carretta, A. Chiesa, and P. Santini, Quantum error correction with molecular spin qudits, Phys. Chem. Chem. Phys. **24**, 20030 (2022).

[71] R. Schutjens, F. A. Dagga, D. J. Egger, and F. K. Wilhelm, Single-qubit gates in frequency-crowded transmon systems, Phys. Rev. A **88**, 052330 (2013).

[72] L. S. Theis, F. Motzoi, and F. K. Wilhelm, Simultaneous gates in frequency-crowded multilevel systems using fast, robust, analytic control shapes, Phys. Rev. A **93**, 012324 (2016).

[73] S. P. Premaratne, J.-H. Yeh, F. C. Wellstood, and B. S. Palmer, Implementation of a generalized controlled-NOT gate between fixed-frequency transmons, Phys. Rev. A **99**, 012317 (2019).

[74] S. E. Economou and E. Barnes, Analytical approach to swift nonleaky entangling gates in superconducting qubits, Phys. Rev. B **91**, 161405(R) (2015).

[75] A. Castro, A. García Carrizo, S. Roca, D. Zueco, and F. Luis, Optimal Control of Molecular Spin Qudits, Phys. Rev. Appl. **17**, 064028 (2022).

[76] M. Atzori, A. Chiesa, E. Morra, M. Chiesa, L. Sorace, S. Carretta, and R. Sessoli, A two-qubit molecular architecture for electron-mediated nuclear quantum simulation, Chem. Sci. **9**, 6183 (2018).

[77] J. Ferrando-Soria, S. Magee, A. Chiesa, S. Carretta, P. Santini, I. Vitorica-Yrezabal, F. Tuna, G. Whitehead, S. Sproules, K. Lancaster, A.-L. Barra, G. Timco, E. McInnes, and R. Winpenny, Switchable interactions in molecular double qubits, Chem **1**, 727 (2016).

[78] For $J_1 = J_2$ only a subset of gaps are nondegenerate. Nevertheless, in combination with universal single-qudit rotations, this constitutes a universal set.

[79] A. Chiesa, P. Santini, D. Gerace, J. Raftery, A. A. Houck, and S. Carretta, Digital quantum simulators in a scalable architecture of hybrid spin-photon qubits, Sci. Rep. **5**, 16036 (2015).

[80] M. K. Wojnar, D. W. Laorenza, R. D. Schaller, and D. E. Freedman, Nickel(II) metal complexes as optically addressable qubit candidates, J. Am. Chem. Soc. **142**, 14826 (2020).

[81] F. Arute, K. Arya, R. Babbush, D. Bacon, J. C. Bardin, R. Barends, S. Boixo, M. Broughton, B. B. Buckley, D. A. Buell, B. Burkett, N. Bushnell, Y. Chen, Z. Chen, B. Chiaro, R. Collins, W. Courtney, S. Demura, A. Dunsworth, E. Farhi *et al.*, Hartree-Fock on a superconducting qubit quantum computer, Science **369**, 1084 (2020).

[82] C. D. Bruzewicz, J. Chiaverini, R. McConnell, and J. M. Sage, Trapped-ion quantum computing: Progress and challenges, Appl. Phys. Lett. **6**, 021314 (2019).

[83] H.-P. Breuer and F. Petruccione, *The Theory of Open Quantum Systems* (Oxford University Press, Oxford, 2010).

[84] W. Yang and R.-B. Liu, Quantum many-body theory of qubit decoherence in a finite-size spin bath, Phys. Rev. B **78**, 085315 (2008).

[85] W. Yang and R.-B. Liu, Quantum many-body theory of qubit decoherence in a finite-size spin bath. II. Ensemble dynamics, Phys. Rev. B **79**, 115320 (2009).